

4-Demethylwyosine Synthase from *Pyrococcus abyssi* Is a Radical-S-adenosyl-L-methionine Enzyme with an Additional [4Fe-4S]⁺ Cluster That Interacts with the Pyruvate Co-substrate*

Received for publication, July 26, 2012, and in revised form, October 3, 2012. Published, JBC Papers in Press, October 5, 2012, DOI 10.1074/jbc.M112.405019

Phan  lie Perche-Letuv  e^{†1}, Velavan Kathirvelu^{‡§¶1}, Gustav Berggren^{‡2}, Martin Clemancey[¶], Jean-Marc Latour[¶], Vincent Maurel[§], Thierry Douki[¶], Jean Armengaud^{**}, Etienne Mulliez[‡], Marc Fontecave^{‡§§}, Ricardo Garcia-Serres^{¶1,3}, Serge Gambarelli^{§4}, and Mohamed Atta^{‡5}

From the [†]Laboratoire de Chimie et Biologie des M  taux,   quipe "Biocatalyse," Institut de Recherches en Technologies et Sciences pour le Vivant, iRTSV-LCBM/Biocat, UMR 5249 Commissariat    l'Energie Atomique (CEA)/CNRS/Universit   Joseph Fourier (UJF), CEA/Grenoble, 17, rue des Martyrs, 38054 Grenoble Cedex 09, France, [§]Laboratoire "R  sonance Magn  tique," UJF-Grenoble 1/CEA/Institut Nanoscience et Cryog  nie/Service de Chimie Inorganique et Biologique (SCIB), UMR-E3, 38054 Grenoble Cedex 09, France, [¶]Laboratoire de Chimie et Biologie des M  taux,   quipe "Physicochimie des M  taux en Biologie," Institut de Recherches en Technologies et Sciences pour le Vivant, iRTSV-LCBM/pmb, UMR 5249 CEA/CNRS/UJF, CEA/Grenoble, 38054 Grenoble Cedex 09, France, [¶]Laboratoire "L  sions des Acides Nucl  iques," UJF-Grenoble 1/CEA/Institut Nanoscience et Cryog  nie/SCIB, UMR-E3, 38054 Grenoble Cedex 09, France, ^{**}Laboratoire de Biochimie des Syst  mes Perturb  s, Service de biochimie et toxicologie nucl  aire, Institut de biologie environnementale et biotechnologie IBEB-SBTN/LBSP F-30207 Bagnols-sur-C  ze, France, and ^{§§}Coll  ge de France, 11 place Marcellin-Berthelot, 75231 Paris Cedex 05, France

Background: 4-Demethylwyosine synthase (TYW1) is a tRNA-modifying metalloenzyme involved in the biosynthesis of wyosine.

Results: TYW1 enzyme belongs to the Radical-SAM superfamily with two Fe-S clusters involved in catalysis.

Conclusion: The canonical Radical-SAM cluster binds and activates SAM co-factor, whereas the additional [4Fe-4S] cluster is shown to interact with the pyruvate co-substrate.

Significance: This study helps to understand how radical-SAM enzymes with two Fe-S centers can synergistically achieve challenging radical insertion reactions.

Wybutosine and its derivatives are found in position 37 of tRNA encoding Phe in eukaryotes and archaea. They are believed to play a key role in the decoding function of the ribosome. The second step in the biosynthesis of wybutosine is catalyzed by TYW1 protein, which is a member of the well established class of metalloenzymes called "Radical-SAM." These enzymes use a [4Fe-4S] cluster, chelated by three cysteines in a CX₃CX₂C motif, and S-adenosyl-L-methionine (SAM) to generate a 5'-deoxyadenosyl radical that initiates various chemically challenging reactions. Sequence analysis of TYW1 proteins revealed, in the N-terminal half of the enzyme beside the Radical-SAM cysteine triad, an additional highly conserved cysteine motif. In this study we show by combining analytical and spectroscopic methods including UV-visible absorption, M  ssbauer, EPR, and HYSCORE spectroscopies that these additional

cysteines are involved in the coordination of a second [4Fe-4S] cluster displaying a free coordination site that interacts with pyruvate, the second substrate of the reaction. The presence of two distinct iron-sulfur clusters on TYW1 is reminiscent of MiaB, another tRNA-modifying metalloenzyme whose active form was shown to bind two iron-sulfur clusters. A possible role for the second [4Fe-4S] cluster in the enzyme activity is discussed.

Post-transcriptional RNA modifications appear to be present in all organisms. Among all RNAs, tRNA contains the broadest repertoire of different modifications and also the highest proportion of modified nucleotides per molecule (1). Functions of tRNAs in translation are enhanced by a series of modifications, and their presence vastly expands the structural and chemical diversity of native tRNA (2). Furthermore, defects in tRNA modification have been linked to several human diseases, underscoring their biological significance (3, 4). All tRNA genes sequenced so far encode a purine (A or G) at position 37, adjacent to the 3' side of the anticodon. After transcription this purine is often enzymatically modified into more complex derivatives, the nature of which depends both on the sequence of the anticodon and the organism. In the case of tRNA^{Phe} three sets of unrelated hyper modifications are reported: N⁶-isopen-tenyladenosine and its derivatives, N⁶-threonylcarbamoylad-

* This work was supported by a GIS (Groupement d'int  r  t scientifique)-CNRS fellowship PP-L, ^{1,2,3}ANR Blanc-2010 Grant INSERAD (to P. P.-L. and V. K.), and R  gion Rh  ne-Alpes Grants CIBLE 2007–2010, 2008–2011, and 2011–2014.

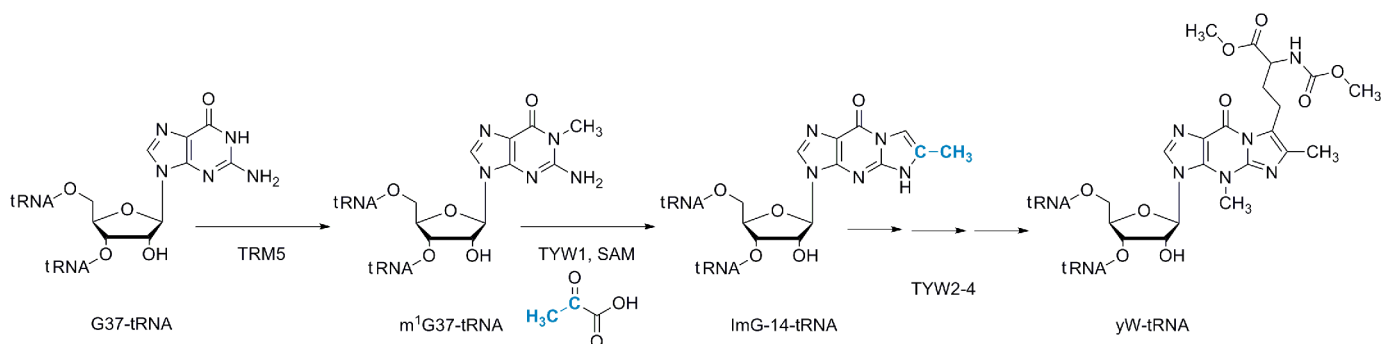
¹ These authors contributed equally.

² Supported by Stiftelsen Bengt Lundqvist minne, the Swedish Research Council FORMAS, and the Royal Swedish Academy of Sciences.

³ To whom correspondence may be addressed. Tel.: 0033438786206; E-mail: ricardo.garcia@cea.fr.

⁴ To whom correspondence may be addressed. Tel.: 0033438783940; E-mail: serge.gambarelli@cea.fr.

⁵ To whom correspondence may be addressed. Tel.: 0033438789115; E-mail: mohamed.atta@cea.fr.



SCHEME 1. Biosynthetic pathway for yW. The enzymes involved in this pathway are: TRM5, TYW1, TYW2, TYW3, and TYW4.

enosine and its derivative, and wyosine (ImG)⁶ derivatives, including wybutosine (yW) (5, 6). The biosynthetic pathway of yW in yeast was revealed recently and shown to be one of the most complex tRNA modification process (7). Indeed a guanosine residue (G37-tRNA) is converted to a tricyclic ¹H-imidazo[1,2- α]purine core structure (Scheme 1) through a multi-enzymatic process depending on five genes (*tyw1–4* and *trm5*) (Scheme 1). The first step of this pathway is committed to methylation of the guanosine residue to *N*¹-methylguanosine (m¹G37, Scheme 1) by the *S*-adenosylmethionine (SAM)-dependent tRNA methyltransferase TRM5. Incorporation of a two-carbon unit into m¹G37-tRNA by TYW1 leads to the formation of the tricyclic base ImG-14-tRNA (Scheme 1), which is further modified by a TYW2, TYW3, and TYW4 multienzyme complex to afford yW. Homologues of TRM5 and TYW1 exist in archaea, suggesting the wide conservation of this reaction pathway from eukaryotes to archaea and the presence of wyosine derivatives in many organisms (8, 9). In this pathway, TYW1 catalyzes an intriguing reaction building a new aromatic ring on the guanine base.

TYW1 belongs to the Radical-SAM enzyme superfamily and like several other members of the family contains two highly conserved motifs of three essential cysteines, both localized at the N-terminal half of the protein (Fig. 1). The CX₃CX₂C motif is the hallmark of the Radical-SAM enzymes responsible for the coordination of a [4Fe-4S] cluster (herein called cluster I) (10), whereas the second motif, CX₁₂CX₁₂C, is present upstream of the Radical-SAM cluster sequence. In Radical-SAM enzymes, SAM binds in a bidentate manner via its α -amino and α -carboxylate groups to the non-cysteinyly-coordinated iron site of this cluster, and in its reduced state, the [4Fe-4S]¹⁺ cluster transfers an electron into the sulfonium group of SAM, inducing its reductive cleavage into L-methionine and a 5'-deoxyadenosyl radical (5'-dA[•]) (11). This radical is used to abstract a hydrogen atom from a specific C-H bond of the substrate that then, in the C[•] radical form, is activated for transformation. In TYW1, the first step is presumed to be an H-atom abstraction from the methyl group of m¹G37-tRNA followed by radical-mediated condensation with a two-carbon-donating species, leading to formation of ImG-14-tRNA. Recently, the identity of this two-carbon-donating species using different labeled puta-

tive precursors has been shown by ms analysis of 4-demethylwyosine to be pyruvate (12).

The native, mostly apo forms of TYW1 enzyme from *Methanococcus jannaschii* and *Pyrococcus horikoshii*, have been crystallized and their structures reported (13, 14). Despite the fact that no electron density for the cluster atoms could be observed in the crystal structure, it was suggested from data collection and phasing statistics that a spatial configuration in which the sulfhydryl groups of the CX₁₂CX₁₂C motif is optimal for chelating another [4Fe-4S] cluster (herein called cluster II). This putative second [4Fe-4S] cluster was shown to be located on the opposite side of the SAM-binding site, and interestingly, its unliganded iron atom faces the inside of this pocket, suggesting a possible role in substrate or co-substrate binding (13).

In this work we demonstrate using a combination of biochemical, analytical, and spectroscopic (light absorption, EPR, HYSCORE, and Mössbauer) methods that TYW1 from the archaeon *Pyrococcus abyssi* contains two [4Fe-4S] clusters. The data presented here strongly suggest that the non-cysteinyly-coordinated iron site of one of the [4Fe-4S] clusters (herein called cluster I) is able in its reduced state to bind SAM, whereas the other [4Fe-4S] cluster (herein called cluster II) interacts with the pyruvate co-substrate. A possible role for the latter [4Fe-4S] cluster in the activity of the enzyme is discussed. This work provides a new example of a Radical-SAM enzyme using its two FeS centers to synergistically achieve difficult radical insertion reactions (15–17).

MATERIALS AND METHODS

Strains—*Escherichia coli* DH5 α was used for plasmid DNA amplification. *E. coli* RosettaTM 2(DE3) host strain (Novagen®, Merck), which contains seven codons rarely used in *E. coli* (AGA, AGG, AUA, CUA, GGA, CCC, and CGG) on a compatible chloramphenicol-resistant plasmid, was used to overexpress the recombinant protein TYW1.

Amino Acid Analysis—Amino acid analysis was performed by Jean-Pierre Andrieu, I.B.S., Grenoble.

Cloning of the TYW1 Gene and Construction of Overexpressing Plasmid—The 972-bp DNA sequence encoding the TYW1 protein was PCR-amplified on a Robocycler gradient 40 (Stratagene) using *P. abyssi* genomic DNA, Pwo polymerase (Roche Applied Science) and the primers 5'-AAGCTAACCCCATATGCCCCGAGGAAGTTGCGAAC-3' and 5'-CAGAAGTGT-TTGCTAAGCTTTAGTTTAAAGGGT-3', designed to contain, respectively, NdeI and HindIII restriction sites. The PCR

⁶ The abbreviations used are: ImG, wyosine; ImG-14, 4-demethyl wyosine; Ado[•], 5'-deoxyadenosyl radical; m¹G, *N*¹-methylguanosine; SAM, *S*-adenosylmethionine; TYW1, 4-demethylwyosine synthase; yW, wybutosine.

Pab	-----MPEEVANLFRKQHYEIVGRHSGVKLCHWLKKSLEGRFCYK	41
Pho	MMEMITIKPGKITVQANPNMPKEVAELFRKQHYEIVGRHSGVKLCHWLKKSLEGRFCYK	60
Af	-----MMNEKLLSELKG--YQIVGKHSVAVKTCWLKKSLEKDEGVCYK	40
Mj	-----MIPEEIIYKILRKQRYQIDG-HTAVKLCGWVRKMLEDKNCYK	41
	: : : : . : : * : * * : . * * * : : : : * * *	
Pab	QKFYGIHSHRCLQMTPLVLAWCTHNCIFCWRPMTFLGTTEL----PQFWDDEPFIVEESIK	97
Pho	QKFYGIHSHRCLQMTPLVLAWCTHNCIFCWRPMENFLGTTEL----PQFWDDEPFIVEESIK	116
Af	QKFYGISCHRCMQMTPAL-MCNQNCILYCWRPLELLKG-----FRGWDEPFIVEESIR	92
Mj	SKFYGIETHRCIQCTPSVIWCQNCIFCWRVLPDIDIGIDISQIKEPKWEEPEVVYKILA	101
	. * * * * * * * : * : * : * * : * : * : * : * : * : * : * : *	
Pab	AQRKLLIGYKGNPK-VDKKKFEEAWPEPKHAAISLSGEPMLYPYMGDLVEEFHKGFTTFI	156
Pho	AQRKLLIGYKGNPK-VDKKKFEEAWNPTHAAISLSGEPMLYPYMGDLVEEFHKGFTTFI	175
Af	AQHRLLSGFHGTG-VNRKKLEEAYEPNQVAISLIGEPITYLPMLELIEEYKKGFTTFI	151
Mj	MHKRIIMGYAGVLDVRGKKFKEALEPKHVAISLSGEPITYLPPYLDLILKIFHKGFTTFV	161
	: : : : * : * * . * * * : * : * : * * * * * : : : : * : * * * * :	
Pab	VTNGTVPERLEEMIKEDKLPQLYVSITAPDIETYSVNI PMIPDGWERIMRFLLEMRDL	216
Pho	VTNGTIPERLEEMIKEDKLPQLYVSITAPDIETYSVNI PMIPDGWERILRFLLEMRDL	235
Af	VTNGTNPDMLEKVK-----PTQLYLSLTADEDSHLVLNRPKGSN-WERVLSLEVMRDS	205
Mj	VSNGLTLDVIEKIE-----PTQLYISLDAYDLDSYRRICG-GKKEYWESILNTLDILKEK	215
	* : * * . : : * : : * * * * : * : * : : : : * * : : . * : : : :	
Pab	PTRTVVRLTLVKGENMHSP--EKYAKLILKARPMFVEAKAYMFVGYSRNRLTINNMPHQ	274
Pho	PTRTVVRLTLVKGENMHSP--EKYAKLILKARPMFVEAKAYMFVGYSRNRLTINNMPHQ	293
Af	GSRTVIRLTLIRGYNMDEEAIRKYSLEIEMAEPDFIEAKAYMYLGYSLRLRLRWGNMPEHA	265
Mj	GRTCIRTTLIRGYNDLIL---KFVELYERADVFIELKSYMHVGYSQRLKEDMLQHD	271
	. * * : * * * : * * . * : : * * * * : * * : * * : * * : * * : *	
Pab	DIREFAEALVKHLPYGHIEDEYEPSRVVLMRDDVDPQGTGVNGRFIKH--	323
Pho	DIREFAEALVKHLPYGHIEDEYEPSRVVLMRDDVDPQGTGVEGRFIKH--	342
Af	DIVEFSRKLADST-GYEVKRESEPSRVVLLER-----VK-----	298
Mj	EILKAKMLDENS-SYKLI DSEDSRVALLQNN-----RKINPKL	311
	: * : : : . * . . * : : : * * * * : * : : : :	

FIGURE 1. Amino acid sequence alignments of TYW1 from (Pab, *P. abyssi*; Af, *Archaeoglobus fulgidus*; Pho, *P. horikoshii*; Mj, *Methanocaldococcus jannaschii*). The alignment was performed with ClustalW at the EBI site. Totally conserved residues are indicated by a star, and conserved cysteine residues are shown in blue boxes.

fragment was then purified by a PCR purification kit (Qiagen), digested by HindIII and NdeI restriction enzymes, and ligated with T4 DNA ligase to NdeI/HindIII-digested pT₇-7 plasmid. Insertion of the TYW1 encoding sequence into the plasmid was controlled by nucleic acid sequencing. The resulting plasmid was named pT₇-TYW1.

TYW1 Overexpression and Purification—RosettaTM 2 (DE3) competent cells were transformed with pT₇-TYW1 plasmid. Selection of the transformants was carried out overnight at 37 °C on a LB-agar plate supplemented with ampicillin and chloramphenicol. From this plate, one colony was used to inoculate LB medium (120 ml) for an overnight culture at 37 °C. Fresh LB medium (12 L) was inoculated with the overnight culture supplemented with antibiotics. Bacteria were grown at 37 °C until $A_{600} = 0.8$, and TYW1 protein overexpression was then induced by the addition of isopropyl-1-thio- β -D-galactopyranoside to a final concentration of 0.5 mM. Cells were further cultivated for 3 h at 37 °C, harvested by centrifugation at $250,000 \times g$ at 4 °C for 20 min, and stored at -70 °C. For extraction and aerobic purification of the protein, cells were first resuspended in a 50 mM Tris-Cl, pH 8, buffer containing 50 mM KCl (3 g of cells/10 ml of buffer) and discontinuously sonicated for 15 min. Cellular extracts were then centrifuged at $250,000 \times g$ for 2 h, and the supernatant was heated at 75 °C for 20 min. Precipitated *E. coli* proteins were eliminated by centrifugation

at $7000 \times g$ for 10 min at 20 °C. Ammonium sulfate was slowly added to the supernatant at 4 °C to a final concentration of 65% (w/v). The solution was stirred for 30 min and centrifuged at $7000 \times g$ for 10 min at 4 °C. The resulting pellet was dissolved in a 50 mM Tris-Cl, pH 8, 50 mM KCl, 1 M ammonium sulfate buffer (buffer A) under stirring. The first chromatographic step was run on a butyl-Sepharose 4 FF column (GE Healthcare, flow rate = 2 ml/min). After washing the column with buffer A, resulting in elution of all nucleic acids and remaining *E. coli* contaminants, TYW1 was eluted with a gradient from 100% buffer A to 100% of buffer B (50 mM Tris-Cl, pH 8, 50 mM KCl). The protein was then desalted on a HiPrep 26/10 desalting column (GE Healthcare) and concentrated using Amicon Centrifugal filters 30 K (Millipore). The apo form of TYW1 was produced by overnight 10 mM EDTA treatment under reducing conditions (2 mM sodium dithionite). ApoTYW1 was then purified on a Superdex S-75 column (GE Healthcare) previously equilibrated with a 50 mM Tris-Cl, pH 8, 50 mM KCl, 5 mM DTT buffer (flow rate = 0.5 ml/min) and concentrated using Amicon Centrifugal filters 30 K.

Protein Purity—Protein purity was assessed by gel electrophoresis by loading 10 μ g of protein on Any kDaTM Mini-Protean[®] TGXTM precast gels (Bio-Rad) with Precision Plus ProteinTM Standards (Bio-Rad). Migration was achieved on a mini-Protean apparatus (Bio-Rad) at 200 V for 25 min.

Reconstitution of the Apo Form of TYW1—Fe-S cluster reconstitution of apoTYW1 was carried out under strictly anaerobic conditions into a Jacomex NT glove box with less than 2 ppm O_2 . After incubation of the apoTYW1 (150 μM) with 5 mM dithiothreitol for 10 min, a 10-fold molar excess of ferrous ammonium sulfate ($Fe(NH_4)_2(SO_4)_2$), or alternatively, a 10-fold molar excess of $^{57}FeSO_4$ was added followed by the addition of a 12-fold molar excess of L-cysteine and a catalytic amount of the *E. coli* cysteine desulfurase CsdA (2% molar equivalent). Evolution of cluster reconstitution was monitored by recording UV-visible spectra every 15 min until absorbance at 410 nm reached a plateau. Holo-TYW1 was then desalted on a NAP-25 cartridge concentrated with Amicon Ultra centrifugal filters 10 K (Millipore).

Preparation of Mössbauer and EPR Samples—EPR and Mössbauer samples (400 μM) were prepared immediately after reconstitution of the clusters. When needed, cluster reduction was achieved in 1 h by the addition of 3 mM dithionite. Samples in presence of SAM and/or pyruvate were prepared with 3 mM SAM and/or pyruvate. Protein-substrate interaction was allowed to proceed for 20 min at 18 °C.

Protein, Iron, Labile Sulfide Concentration Assays—Holo-TYW1 protein concentration was determined by Bradford assay and quantitative amino acid analysis ($\epsilon_{280} = 116 \text{ mM}^{-1} \cdot \text{cm}^{-1}$). Compared with amino acid analysis, standard Bradford assay calibrated with bovine serum albumin overestimated the holo-TYW1 concentration by a factor of 1.3. Protein-bound iron was determined by a modified Fish procedure (18). Labile sulfide was determined according to standard procedure (19).

Yeast tRNA Preparation—Haploid yeast strain BYK4742Kan Δ Ypl207w was cultivated overnight at 30 °C on a YPD-agar plate. From this plate, a 100-ml overnight culture in YPD medium (2% glucose, 1% yeast extract) was prepared and used to inoculate 5 liters of fresh YPD medium. At $A_{600} = 10$, cells were harvested by centrifugation (55 g) and suspended in 55 ml of 10 mM Tris-Cl, pH 7.4, 10 mM $MgCl_2$, 150 mM NaCl buffer. One volume of phenol was added, and the mixture was slowly shaken and incubated 30 min at room temperature. Cells were then centrifuged at $1500 \times g$ for 10 min at room temperature. The supernatant was washed once with 1 volume of phenol. The aqueous phase was separated by centrifugation at $7000 \times g$ for 10 min at room temperature. tRNAs were then precipitated for 2 h at $-20^\circ C$ with 0.7 volume of cold isopropyl alcohol. After centrifugation at $7000 \times g$ for 10 min at $4^\circ C$, the pellet was rinsed with 5×1 ml of 70% cold ethanol, dried, and solved in 12 ml of 10 mM Tris-Cl, pH 7.4, 10 mM $MgCl_2$, 150 mM NaCl buffer. Bulk tRNAs were purified on a Nucleobond AX10000 column (Macherey NagelTM) and precipitated by 0.7 volume of isopropyl alcohol at $-20^\circ C$ overnight. After centrifugation at $7000 \times g$ for 10 min at $4^\circ C$, the pellet was rinsed with 3×1 ml of 70% cold ethanol, dried and solved in sterile water. Concentration of tRNAs was measured on a Nanodrop spectrophotometer ND-100 (Labtech) by measuring absorbance at 260 nm considering that $1 A_{260} \text{ unit} = 40 \mu g$ of tRNAs.

In Vitro Activity Assays—Assays were carried-out in an anaerobic chamber. Experiments were performed in 0.1 M Tris-Cl, pH 8, 0.1 M KCl with 200 μg of yeast tRNAs. The assay

mixtures contained fixed concentrations of sodium dithionite (2 mM), pyruvate (1 mM), and SAM (1 mM). Variable amounts of holo-TYW1 (0–20 μM) were tested. Except for kinetic studies, reactions were performed at 60 °C for 30 min and quenched by opening samples to air and acidification of the mixture to pH 6 by a 3.5 M acetate buffer, pH 4.5. tRNAs were then digested to nucleosides and analyzed by HPLC as described below.

Analysis of tRNA Nucleoside Composition by HPLC—Yeast tRNAs and the *in vitro* assay solutions (100–200 μg of tRNAs) were digested overnight to nucleosides by nuclease PI (Nuclease 5'-Nucleotidehydrolase, 3'-Phosphohydrolase) and Phosphodiesterase II at pH 6, 37 °C, after the addition of 1 mM $Zn(OAc)_2$. After buffering to pH 8, samples were digested by bacterial alkaline phosphatase (Sigma) and phosphodiesterase I for 3 h. tRNA solutions were then injected onto Zorbax SB-C18 column connected to a HP-1100 HPLC system. The high resolution HPLC-UV method developed by Gehrke and Kuo (20) was used to analyze the nucleoside composition of samples.

HPLC-Mass Spectrometry Analyses of tRNA—Aliquot fractions of enzymatically hydrolyzed tRNAs were injected on a HPLC series 1100 (Agilent) equipped with a 2×150 -mm inner diameter (particle size 5 μm) reverse phase column (Uptisphere ODB, Interchim, Montluçon, France). The separation involved a gradient of methanol in a 2 mM ammonium formate aqueous solution. The outlet of the column was connected to the ionization chamber of an API 3000 triple quadrupolar mass spectrometer (AB Sciex) operated in the positive ionization mode. In a first series of analyses, pseudomolecular ions specifically corresponding to m^1G ($m/z = 299$) and $ImG-14$ ($m/z = 322$) were detected. The mass spectrum corresponding to the retention times of the two compounds was then recorded. Finally, fragmentation mass spectra involving use of the mass spectrometer in the ion monitoring modes were obtained.

Analysis of the Fate of Pyruvate in the Presence of Reduced Holo-TYW1—In an anaerobic chamber, as described above, holo-TYW1 (400 μl , 380 μM) in 50 mM Tris-Cl, pH 8, 100 mM KCl was reduced by sodium dithionite (3 mM) for 1 h during which time the reduction was monitored by the decrease in absorption at 410 nm. Once the reduction was complete, the reaction solution was desalted on a NAP-10 cartridge to remove any residual dithionite and concentrated to 200 μl (480 μM) with Amicon Ultra centrifugal filters 10 K (Millipore). The purified reduced protein was treated with pyruvate (3 mM), and the reaction was allowed to proceed for 15 min before aliquots were flash-frozen in liquid nitrogen. The aliquots were thawed, diluted 1:10 with H_2O , acidified using 2 M H_2SO_4 , and taken out of the glove box for injection onto a Rezex ROA-Organic Acid H^+ (Phenomenex) column connected to a HP-1100 HPLC system. Samples were analyzed by an isocratic flow protocol (buffer 5 mM H_2SO_4 (aqueous)). These conditions allow for the detection of by-products such as lactate, formate, or acetate.

UV-Visible Spectroscopy—Aerobic UV-visible data were recorded on a UV-1800 spectrophotometer (Shimadzu). Anaerobic UV-visible spectra were recorded on an Uvikon XL100 spectrophotometer (Bio-Tek instruments) connected by optical fibers to the cuvette holder in the anaerobic chamber.

EPR and HYSCORE Spectroscopies—EPR spectra were recorded on a Bruker EMX spectrometer operating at X band

frequency equipped with an Oxford instrument ESR 900 flow cryostat. Spectra were recorded at 8 K with microwave frequency 9.65 GHz, power at 24 db, modulation amplitude at 5 G, simulated with Easy Spin toolbox for matLAB.

HYSCORE experiments were performed on a Bruker Elexsys E-580 X-band pulsed spectrometer with a Bruker ER4118X dielectric resonator and a continuous flow He cryostat (Oxford Instrument CF935) controlled by an Oxford Instrument temperature controller ITC 503. Experiments were performed at 10 K using the standard four-pulse sequence ($\pi/2$ - τ - $\pi/2$ - t_1 - π - t_2 - $\pi/2$ -echo) with a nominal pulse width of 16 ns for $\pi/2$ and 32 ns for π pulses, a τ value of 132 ns, and a shot repetition rate of 1 kHz. Unwanted echoes were removed by four-step phase cycling. A 128×128 dataset was recorded with times t_1 and t_2 incremented in 24-ns steps from an initial value of 200 ns. This dataset was processed using Xepir software (Bruker). The background decay in both dimensions was subtracted using a linear fit followed by apodization with a Hamming window and 0-fill-ing to 512 points in each dimension. The two-dimensional Fourier transform magnitude spectrum was calculated and presented as a contour plot. The isotropic hyperfine coupling constant of interacting nitrogen was obtained from double quantum-double quantum correlation signal using the standard relation

$$\nu_{dq\pm} = 2[(\nu_N + |a_N|/2)^2 + K^2(3 + \eta^2)]^{1/2}$$

where ν_N is the nuclear Zeeman frequency, a_N is isotropic hyperfine coupling constant, K is the quadrupole coupling constant, and η is the asymmetry parameter (21).

Mössbauer Spectroscopy—Mössbauer spectra were recorded at 4.2 K either on a low field Mössbauer spectrometer equipped with a Janis SVT-400 cryostat or on a strong field Mössbauer spectrometer equipped with an Oxford Instruments Spectromag 4000 cryostat containing an 8-tesla split-pair superconducting magnet. Both spectrometers were operated in a constant acceleration mode in transmission geometry. The isomer shifts were referenced against that of a room temperature metallic iron foil. Analysis of the data were performed with the program WMOSS (WEB Research).

Background-subtracted Mössbauer spectra were generated according to the following procedure; a spectrum of a holo-TYW1 sample with high $[4\text{Fe-4S}]^{2+}$ cluster content (95% of total iron) was fit with a quadrupole doublet (see Fig. 2). For each preparation of a holo-TYW1 sample with a co-substrate, a reference sample of holo-TYW1 was collected, and its $[4\text{Fe-4S}]^{2+}$ cluster content was estimated using the same theoretical spectrum. This theoretical spectrum scaled to the estimated % absorption was then subtracted from the experimental spectrum. The difference spectrum thus obtained was used as a “residual” to be subtracted from the raw data of other samples stemming from the same batch, thus allowing to follow the fate of the initial $[4\text{Fe-4S}]^{2+}$ clusters.

RESULTS

Cloning, Expression, and Purification of *P. abyssi* TYW1 Protein—The *tyw1* gene of *P. abyssi* was cloned into the NdeI and HindIII sites of expression vector pT₇-7 by standard meth-

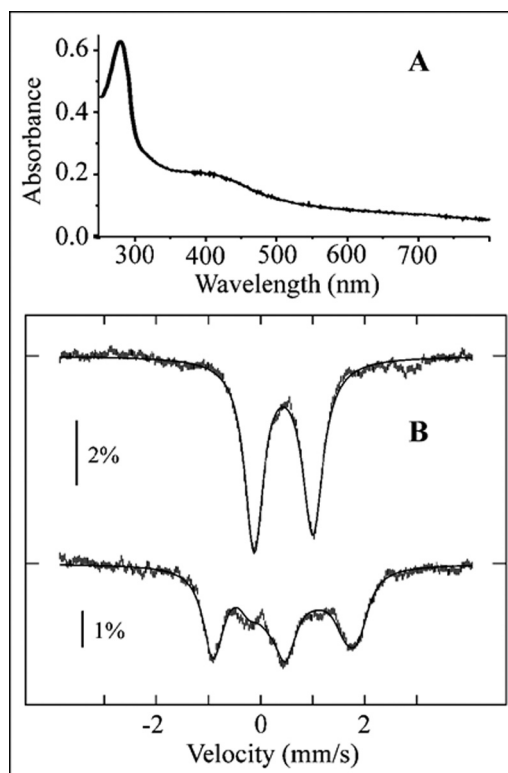


FIGURE 2. UV-visible and Mössbauer spectra of as-reconstituted holo-TYW1. Panel A, UV-visible spectra of holo-TYW1 (5.6 μM) in 50 mM Tris-Cl, pH 8, containing 50 mM KCl are shown. Panel B, a Mössbauer spectrum of holo-TYW1 (400 μM) reconstituted with ^{57}Fe in the same buffer is shown. Experimental spectra (hatched marks) were recorded at 4.2 K in a magnetic field of 600 G (top) or 6 T (bottom), applied parallel to the direction of the γ -beam. The solid line overlaid with the low-field spectrum is a quadrupole doublet simulation with parameters given in the text (“Spectroscopic Characterization of Holo-TYW1 in the Oxidized State”). The solid line overlaid with the 6-tesla spectrum represents a spin Hamiltonian simulation assuming an $S = 0$ ground state and the aforementioned quadrupole parameters with an asymmetry parameter $\eta = 0.07$.

ods. The obtained pT₇-TYW1 plasmid was introduced into *E. coli* Rosetta 2 strain, which resulted in the overproduction of a protein migrating at ~ 37 kDa on SDS gels, in good agreement with the molecular mass deduced from amino acid sequence (37.8 kDa). The expressed protein was found mainly in the soluble fraction of cell-free extracts. After the final step of purification, the purity was evaluated by SDS-PAGE to be over 95% (Data not shown). Quantitative amino acid analysis, employed to establish an extinction coefficient for holo-TYW1, showed that the Bradford assay, using BSA as a standard, overestimates the concentration of the protein by a factor of 1.3. The as-purified protein was light-brown in color and found to contain low amounts of both iron and sulfur atoms (<0.7 iron, sulfur per monomer). This suggested the presence of a protein-bound iron-sulfur cluster, however, in substoichiometric amounts, probably as a consequence of cluster loss during aerobic purification. Anaerobic treatment of the protein solution with an excess of ferrous iron and enzymatically produced sulfide generated a holo-TYW1 protein which after desalting contained up to 8.2 ± 0.2 iron and 8.2 ± 1.6 sulfide ions per polypeptide chain, suggesting the presence of two $[4\text{Fe-4S}]$ clusters per polypeptide.

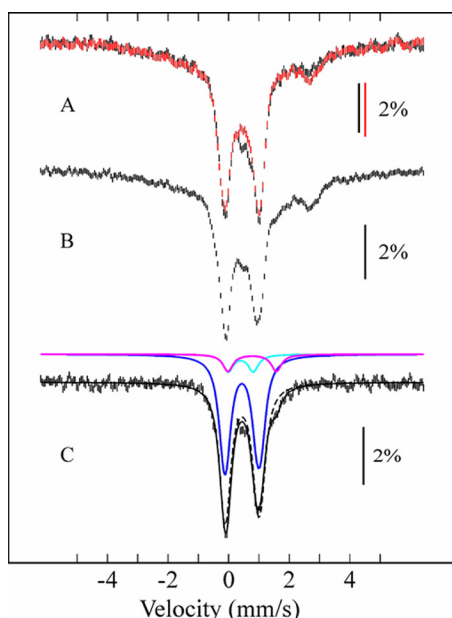


FIGURE 3. Mössbauer spectra of holo-TYW1 (A, black marks), holo-TYW1 incubated with SAM (A, red marks), and holo-TYW1 incubated with SAM and pyruvate (B and C). The experimental spectra (hatched marks) were recorded at 4.2 K in a magnetic field of 600 G applied parallel to the direction of the γ -beam. In C, residual spectra originating from species other than $[4\text{Fe-4S}]^{2+}$ clusters have been subtracted from the raw data according to the procedure described in the methods section. The resulting spectrum was fit with three quadrupole doublets corresponding to holo-TYW1 (blue line, 78%, $\delta = 0.44 \text{ mm}\cdot\text{s}^{-1}$, $\Delta E_Q = 1.13 \text{ mm}\cdot\text{s}^{-1}$), the ferrous site of a localized pair (purple line, 8%, $\delta = 0.78 \text{ mm}\cdot\text{s}^{-1}$, $\Delta E_Q = +1.62 \text{ mm}\cdot\text{s}^{-1}$), and its ferric counterpart (cyan line, 8%, $\delta = 0.38 \text{ mm}\cdot\text{s}^{-1}$, $\Delta E_Q = +0.81 \text{ mm}\cdot\text{s}^{-1}$). The solid black line overlaid on the experimental data points is a composite spectrum obtained by summing these three components. The dotted black line illustrates the misfit to the data when not adding a differentiated site.

Spectroscopic Characterization of Holo-TYW1 in the Oxidized State—The UV-visible spectrum of holo-TYW1 in the fully oxidized state is displayed in Fig. 2A. It comprises a broad shoulder centered at 410 nm that is characteristic of $[4\text{Fe-4S}]^{2+}$ clusters and has an A_{410}/A_{280} ratio = 0.33 suggesting a full occupancy of the clusters. Moreover, the molar extinction coefficient at 410 nm ($\epsilon_{410} = 34.5 \text{ mM}^{-1}\cdot\text{cm}^{-1}$) is consistent with the presence of two $[4\text{Fe-4S}]^{2+}$ clusters per holo-TYW1, as biological $[4\text{Fe-4S}]^{2+}$ centers typically have $\epsilon_{410} = 15\text{--}17 \text{ mM}^{-1}\cdot\text{cm}^{-1}$ on a per cluster basis.

Fig. 2B, top, presents the Mössbauer spectrum of holo-TYW1 reconstituted with ^{57}Fe and recorded at 4 K with a small magnetic field applied parallel to the γ -rays. It is mostly constituted by one asymmetric quadrupole doublet that accounts for $\sim 95\%$ of total iron. This doublet can be simulated with parameters ($\delta = 0.44 \text{ mm}\cdot\text{s}^{-1}$, $\Delta E_Q = 1.13 \text{ mm}\cdot\text{s}^{-1}$) indicative of iron centers in $[4\text{Fe-4S}]^{2+}$ clusters, and this assignment is supported by the high-field spectrum illustrated in Fig. 2B, bottom, that reveals an $S = 0$ ground state. Because titrations indicate the presence of 8.2 ± 0.2 iron and 8.2 ± 1.6 sulfide per polypeptide chain and $\epsilon_{410} = 34.5 \text{ mM}^{-1}\cdot\text{cm}^{-1}$, we safely conclude that each holo-TYW1 polypeptide chain contains two $[4\text{Fe-4S}]^{2+}$ clusters, as suggested by Nureki and co-workers (13).

When a sample of holo-TYW1 was incubated for 20 min with SAM, no significant change could be detected in the Mössbauer spectrum (Fig. 3A). However, after further addition of pyruvate to this sample, a shoulder developed at high velocity (Fig. 3, B

and C). This shoulder may correspond to the high energy line of a quadrupole doublet accounting for 8% of the iron assigned to $[4\text{Fe-4S}]^{2+}$ clusters. Simulation of the data with the same parameters without accounting for a new specific site yields a misfit (Fig. 3C, dotted line). The new doublet displays parameters ($\delta = 0.78 \text{ mm}\cdot\text{s}^{-1}$, $\Delta E_Q = +1.62 \text{ mm}\cdot\text{s}^{-1}$) similar to those of the unique site of aconitase bound to its substrate citrate ($\delta = 0.84 \text{ mm}\cdot\text{s}^{-1}$, $\Delta E_Q = +1.26 \text{ mm}\cdot\text{s}^{-1}$) or isocitrate ($\delta = 0.89 \text{ mm}\cdot\text{s}^{-1}$, $\Delta E_Q = +1.83 \text{ mm}\cdot\text{s}^{-1}$) (22). We thus tentatively assign it to a $[4\text{Fe-4S}]$ -pyruvate complex. Experiments under high applied magnetic fields reveal a diamagnetic ground state. This supports the assignment of this doublet as the “more ferrous” center of a localized $\text{Fe}^{\text{II}}\text{Fe}^{\text{III}}$ pair belonging to a $[4\text{Fe-4S}]^{2+}$ cluster with a unique iron site. Subtraction of the spectrum of holo-TYW1 after scaling reveals a second doublet consistent with the ferric center of this localized pair. The spectrum was, therefore, fitted with three quadrupole doublets corresponding to: doublet used for holo-TYW1 (blue line, 78%, $\delta = 0.44 \text{ mm}\cdot\text{s}^{-1}$, $\Delta E_Q = 1.13 \text{ mm}\cdot\text{s}^{-1}$), ferrous site of localized pair (purple line, 8%, $\delta = 0.78 \text{ mm}\cdot\text{s}^{-1}$, $\Delta E_Q = +1.62 \text{ mm}\cdot\text{s}^{-1}$), and ferric site of localized pair (cyan line, 8%, $\delta = 0.38 \text{ mm}\cdot\text{s}^{-1}$, $\Delta E_Q = +0.81 \text{ mm}\cdot\text{s}^{-1}$). The pyruvate-interacting cluster accounts for 32% ($4 \times 8\%$) of all $[4\text{Fe-4S}]^{2+}$ clusters, which means that about two-thirds of all proteins could be interacting with pyruvate in these conditions.

Spectroscopic Characterization of Holo-TYW1 in the Reduced State—Upon the addition of dithionite on the reconstituted holo-TYW1, the absorption decreased over the entire 310–420-nm range (Fig. 4A), as expected for the conversion of the $S = 0$ $[4\text{Fe-4S}]^{2+}$ chromophore to the $S = 1/2$ $[4\text{Fe-4S}]^{1+}$ level. This reduced form has been investigated by X-band EPR and HYSCORE spectroscopies. The CW (continuous wave) EPR spectrum of the dithionite-reduced holo-TYW1 protein is depicted in Fig. 4B, top. This spectrum is complex and cannot be simulated with a single rhombic g tensor, suggesting that more than one species contributes to the spectrum. The addition of SAM to the reduced holo-TYW1 induced a substantial change in the resonance position and shape of EPR spectrum (Fig. 4B, middle). It also provides a clear evidence for the existence of two different species that could be readily identified. Further treatment of the reduced holo protein with pyruvate (Fig. 4B, bottom) led to the disappearance of a set of transitions marked by asterisks in Fig. 4B, middle, which simplifies the EPR spectrum to a large extent. These observations can be explained as follows by considering that the holo protein possesses two $[4\text{Fe-4S}]$ clusters that interact independently with SAM and pyruvate. The complex EPR spectrum of the reduced holo-TYW1 is attributed to the superimposition of the signals from two $[4\text{Fe-4S}]^{1+}$ clusters with $S = 1/2$ spins (Fig. 4B, top). Even though the presence of some impurity signal complicates the analysis, the EPR spectrum could be simulated satisfactorily by considering the following two sets of principal g values: 1.858(9), 1.895(3), and 2.023(1) for cluster I and 1.842(9), 1.926(4), 2.054(6) for cluster II in the ratio of 2:1. The EPR spectrum of SAM-treated reduced holo protein could be well fitted again by considering two clusters with the principal g values of 1.827(2), 1.858(2), 1.977(1) for cluster I and 1.828(6), 1.932(2), 2.055(2) for cluster II in the ratio of 2.8:1. Comparison

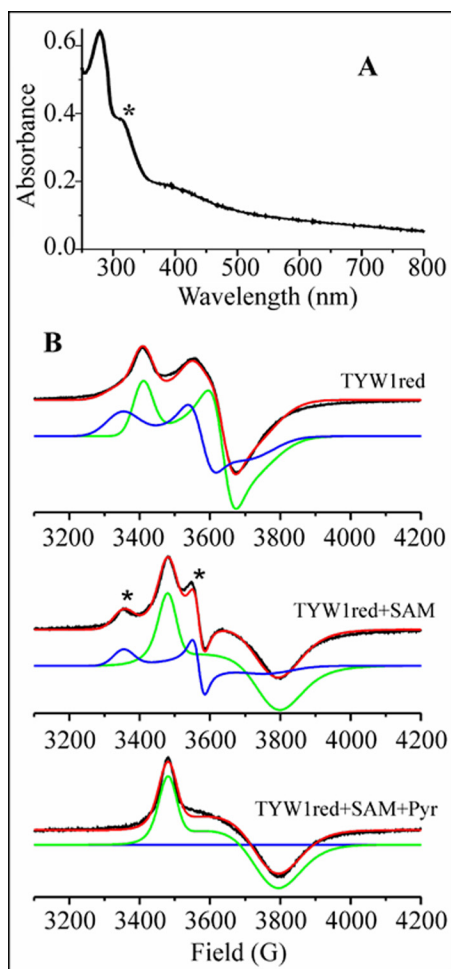


FIGURE 4. UV-visible and EPR spectra of reduced holo-TYW1. Panel A, UV-visible spectra of reduced holo-TYW1 (5.6 μM) in 50 mM Tris-Cl, pH 8, containing 50 mM KCl; the asterisk corresponds to the absorption of dithionite. Panel B, shown is an EPR spectrum of reduced holo-TYW1 (400 μM) incubated with 3 mM dithionite (top), 3 mM SAM (middle), and 3 mM SAM and 3 mM pyruvate (bottom). Black traces are experimental spectra recorded at 8 K, $\nu = 9.65$ GHz, power 24 dB, modulation amplitude 5 G. The top red trace is the sum of individual components simulated with $S = 1/2$ using g values 1.858(9), 1.895(3), 2.023(1) for cluster I (green) and 1.842(9), 1.926(4), 2.054(6) for cluster II (blue) in the ratio of 2:1; the middle red trace is the sum of individual components simulated with $S = 1/2$ using g values 1.827(2), 1.858(2), 1.977(1) for cluster I (green) and 1.828(6), 1.932(2), 2.055(2) for cluster II (blue) in the ratio of 2.8:1; and the bottom red trace is simulated solely with cluster I (green) using g values 1.827(2), 1.858(2), 1.977(1).

of these values with those of the reduced holo-TYW1 shows that cluster II is unaffected by SAM addition, which by contrast drastically alters the EPR spectrum of cluster I. This indicates that (i) there is a specific interaction between SAM and cluster I, and (ii) all clusters I in the reduced holo-TYW1 interact with SAM.

The interaction of SAM with cluster I was further evidenced by performing a HYSORE experiment (Fig. 5). Indeed, the HYSORE spectrum of the anaerobically reduced holo-TYW1 presented no cross-correlation peaks in the $(-, +)$ quadrant. In the $(+, +)$ quadrant, only peaks from distant ^{13}C carbon atoms present in natural abundance are observed (Fig. 5A). Upon the addition of SAM to an anaerobic solution of holo-TYW1 in the reduced form, the HYSORE spectrum was drastically modified (Fig. 5B) and a symmetrical set of new features appeared in

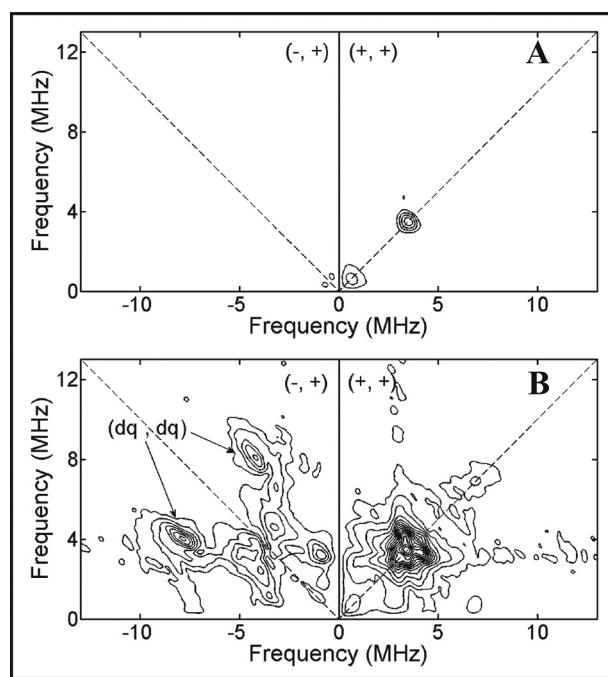


FIGURE 5. HYSORE spectra of the anaerobically reduced holo-TYW1 (400 μM) before (recorded at $g = 1.908$) (A) and after (recorded at $g = 1.837$) the addition of 3 mM of SAM (B).

the $(-, +)$ quadrant. These peak patterns and their positions are characteristic of a strongly coupled nitrogen atom ($|a_{\text{N}}|/2 \gg \nu_{\text{N}}$, an $I = 1$ nucleus with quadrupolar coupling). The strong cross-peak pair centered at -4 ± 0.1 , 8 ± 0.1 and 4 ± 0.1 , -8 ± 0.1 in the $(-, +)$ quadrant are assigned to double quantum-double quantum correlation. The first order analysis of the double quantum correlation frequency yields an isotropic hyperfine coupling ($|a_{14\text{N}}| = 5.6$ MHz, which is very close to those obtained by HYSORE spectroscopy for anaerobic ribonucleotide reductase activating enzyme ($|a_{14\text{N}}| = 6.4$ MHz) (23), spore photoproduct lyase ($|a_{14\text{N}}| = 6.5$ MHz) (24), and by ^{15}N ENDOR spectroscopy of lysine 2,3-aminomutase ($|a_{15\text{N}}| = 9.1$ MHz) (25). This strongly suggests that the amino group of SAM is coordinated to the unique iron of the $[\text{4Fe-4S}]^{1+}$ center I of holo-TYW1 in a manner similar to that demonstrated in these enzymes.

As indicated above, further addition of pyruvate to this sample strongly affects and simplifies the CW EPR spectrum that can now be simulated with a single set of the principal g values associated to the cluster I-SAM complex. This indicates that the contribution of cluster II has been abolished by pyruvate addition. Two hypotheses can be put forward to account for this observation; (i) an interaction of pyruvate with cluster II could cause the signal to spread over a large field and broaden beyond detection, or (ii) this hypothetical interaction could induce the oxidation of cluster II to the EPR silent $S = 0$ $[\text{4Fe-4S}]^{2+}$ state.

To probe these hypotheses two samples of the reduced ^{57}Fe -enriched holo-TYW1 incubated either with SAM or with SAM and pyruvate were analyzed by Mössbauer spectroscopy. The spectrum of the "SAM sample" was subtracted from that of the "SAM+pyruvate sample" to eliminate the contributions of the reduced species, and the resulting spectrum is shown in Fig.

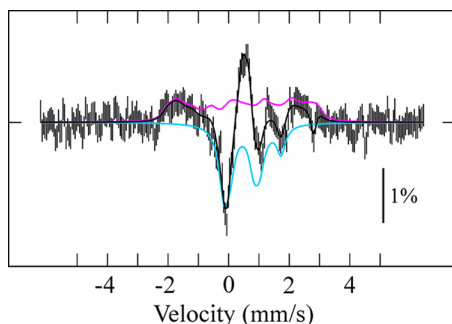


FIGURE 6. Mössbauer difference spectrum (hatched marks) obtained by subtracting the raw spectrum of dithionite-reduced holo-TYW1 incubated with SAM from that of dithionite-reduced holo-TYW1 incubated with SAM and pyruvate. The black solid line represents the theoretical composite spectrum obtained by summing a positive contribution of 16% of total iron from a $[4\text{Fe-4S}]^{2+}$ cluster with a differentiated iron site (blue line), a negative contribution of 14% of total iron from a $[4\text{Fe-4S}]^{1+}$ cluster (pink line), and minor contributions from unbound Fe^{II} (not plotted). The raw experimental spectra were recorded at 4.2 K in a magnetic field of 600 G applied parallel to the direction of the γ -beam.

6. The plotted simulation (black line) involves a negative contribution (14% of total iron) with parameters characteristic of $[4\text{Fe-4S}]^{1+}$ clusters (pink line) and a positive contribution (16% of total iron) corresponding to a $[4\text{Fe-4S}]^{2+}$ cluster with a differentiated iron site (blue line) as well as minor contributions of unbound Fe^{II} (not plotted). The negative contribution from $[4\text{Fe-4S}]^{1+}$ clusters (pink line) was simulated with spin-Hamiltonian parameters typical for $S = 1/2$ $[4\text{Fe-4S}]^{1+}$ cluster proteins. This shows that pyruvate addition to the reduced holo-TYW1 protein in the presence of SAM does not only alter the environment of cluster II unique site but also induces the re-oxidation of cluster II. To shed light on whether the suggested re-oxidation of the second cluster is connected to chemical transformation of pyruvate, the reduced holo-TYW1 protein was incubated for 15 min in presence of pyruvate, and the resulting solution was analyzed by HPLC (data not shown). Under these experimental conditions, neither a decrease in pyruvate concentration nor formation of metabolites (e.g. neither lactate, which is the primary product expected for pyruvate reduction, nor formate, nor acetate) could be detected.

Conversion of $m^1\text{G37-tRNA}$ to ImG-14-tRNA Catalyzed by Holo-TYW1 Protein *In Vitro*—To investigate the enzymatic conversion of $m^1\text{G37-tRNA}$ to ImG-14-tRNA *in vitro*, we extracted a tRNA substrate from a *Saccharomyces cerevisiae* strain lacking a functional *tyw1* gene. The purified bulk tRNAs from this strain were digested and analyzed for their modified nucleosides content by HPLC as previously described (20). As shown in Fig. 7A, the peak eluting at 32.9 min was identified as the $m^1\text{G37-tRNA}$ modification. This assignment was confirmed by UV-visible spectrum (Fig. 7B) and mass spectrometry (Fig. 7C). This analysis also confirmed the absence of the yW base known to elute at 65 min (20). The tRNAs isolated from this strain contains increased amounts of $m^1\text{G37-tRNA}$, the substrate of TYW1, and was named $m^1\text{G37-tRNA}$.

To assay the reconstituted TYW1, we established standard reaction conditions. Typically, the reaction mixture (150 μl) contained reconstituted TYW1, $m^1\text{G37-tRNA}$, SAM, dithionite, and pyruvate in 50 mM Tris-Cl, pH 8. The reaction was carried out at 60 °C for 30 min under anaerobic conditions then

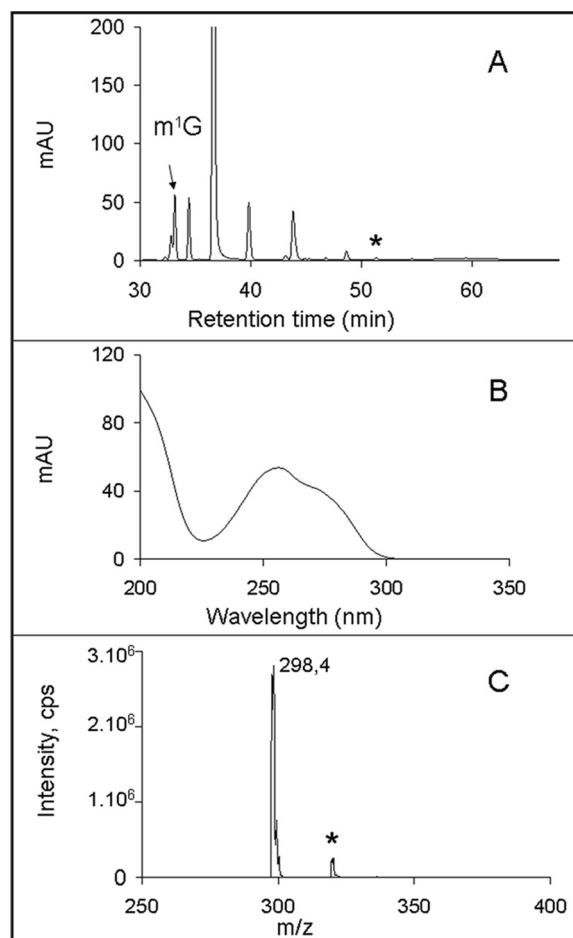


FIGURE 7. HPLC, UV-visible, and mass spectra of $m^1\text{G}$ -modified nucleoside. Panel A, shown is a HPLC chromatogram of the 30–68-min region of digested bulk tRNA (100 μg) from *S. cerevisiae* Δtyw1 ; $m^1\text{G}$ is shown by an arrow and elutes at 32.9 min. Panel B, shown is a UV-visible spectrum of the peak at 32.9 min. Panel C, mass spectrometry detection was carried out in neutral loss mode to obtain a high specificity as described under “Materials and Methods.” The main peak corresponds to the mass of protonated $m^1\text{G}$ -modified nucleoside ($\text{MH}^+ = 298.4$). The peak with the asterisk corresponds to the Na^+ -adduct pseudomolecular ions for $m^1\text{G}$ ($\text{M} + \text{Na}^+ = 320.3$). mAU, milliabsorbance units.

stopped by opening the mixture to air and brought to pH 6. tRNAs were completely hydrolyzed by nuclease P1 and alkaline phosphatase, and the resulting hydrolysate was analyzed by HPLC. The analyses are presented in Fig. 8.

HPLC chromatogram (Fig. 8A) showed a new peak eluting at 51.9 min corresponding to the ImG-14 nucleoside. This was confirmed by both mass spectrometry (Fig. 8B) and UV-visible spectroscopy (Fig. 8C) in agreement with previously published UV-visible spectrum (26). It is worth noticing that this new peak corresponding to ImG-14 co-elutes with a contaminant also present in the control experiment and $m^1\text{G37-tRNA}$ (asterisks on Figs. 7A and 8D). This contaminant has different UV spectroscopic properties from ImG-14 (Fig. 8E).

No ImG-14 could be detected when the TYW1 protein, SAM, dithionite, or pyruvate was omitted from the reaction mixture (Fig. 8D). The HPLC chromatograms (Fig. 8, A and D) also showed two new peaks appearing at retention times of 35.2 min and 35.7 min (filled squares on Fig. 8D). These peaks can be safely attributed to SAM derivatives as they only appear in the

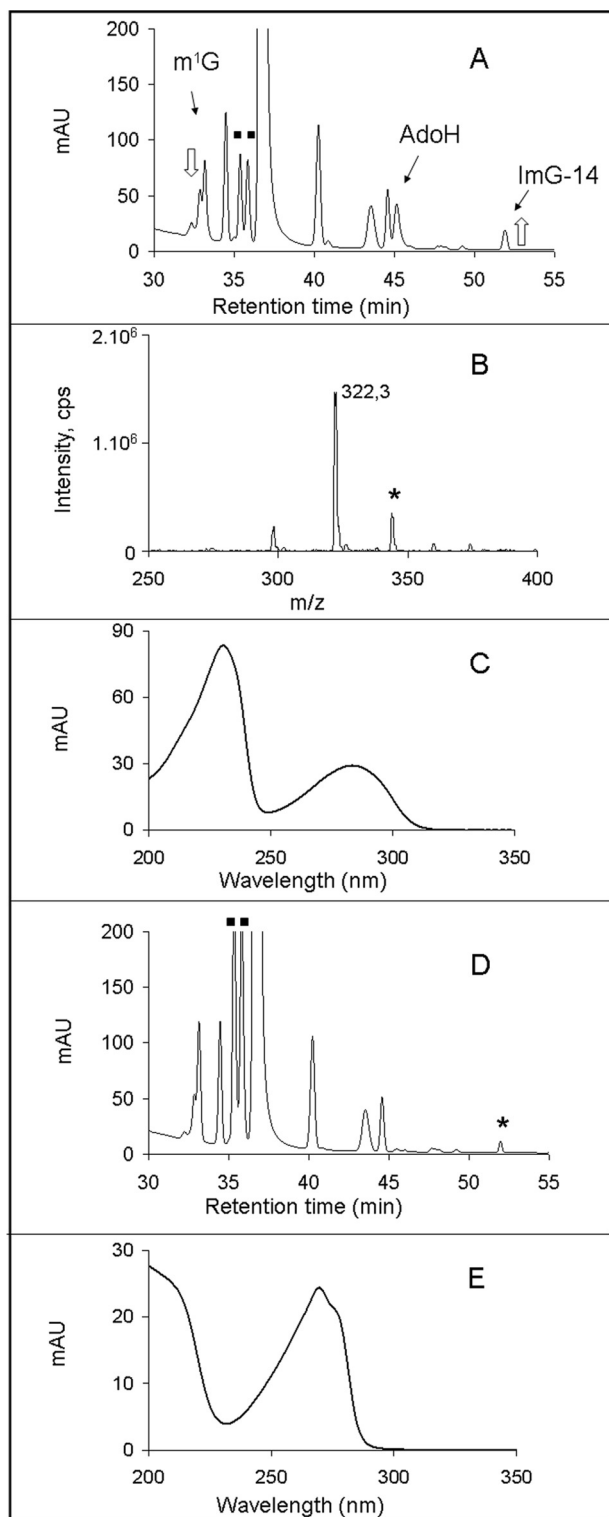


FIGURE 8. HPLC, UV-visible, and mass spectra of ImG-14-modified nucleoside from *in vitro* assay. Panel A, shown is a HPLC chromatogram of digested tRNAs (200 μ g) from the *in vitro* assay conducted with 20 μ M TYW1, 1 mM SAM, 1 mM pyruvate, 1 mM dithionite for 30 min at 60 °C. A down arrow (\downarrow) indicates a decrease in m¹G peak area (32.9 min). The up arrow (\uparrow) indicates an increase of peak area at 51.9 min corresponding to ImG-14 formation. Filled squares indicate two new peaks that correspond to SAM derivatives. mAU, milliabsorbance units. AdoH, 5'-deoxyadenosine. Panel B, shown is a mass spectrum of the peak at 51.9 min corresponding to ImG-14. The main peak corresponds to the mass of protonated ImG-14-modified nucleoside ($MH^+ = 322.4$). The peak with the asterisk corresponds to the Na⁺-adduct pseudomolecular ions for ImG-14 ($M + Na^+ = 344.3$). Panel C, shown is a UV-

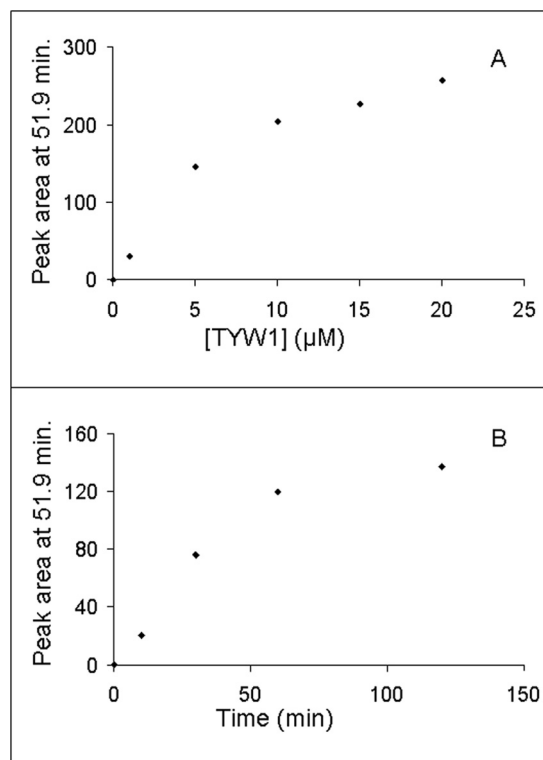


FIGURE 9. Evolution of peak area at 51.9 min associated to ImG-14 formation. Panel A, peak area is shown as a function of TYW1 concentration in a 30-min assay. Panel B, peak area is shown as a function of time (TYW1 concentration = 2 μ M). Both experiments were conducted at 60 °C in the presence of 1 mM SAM, 1 mM pyruvate, and 2 mM dithionite in Tris-Cl 50 mM, pH 8, containing 50 mM KCl.

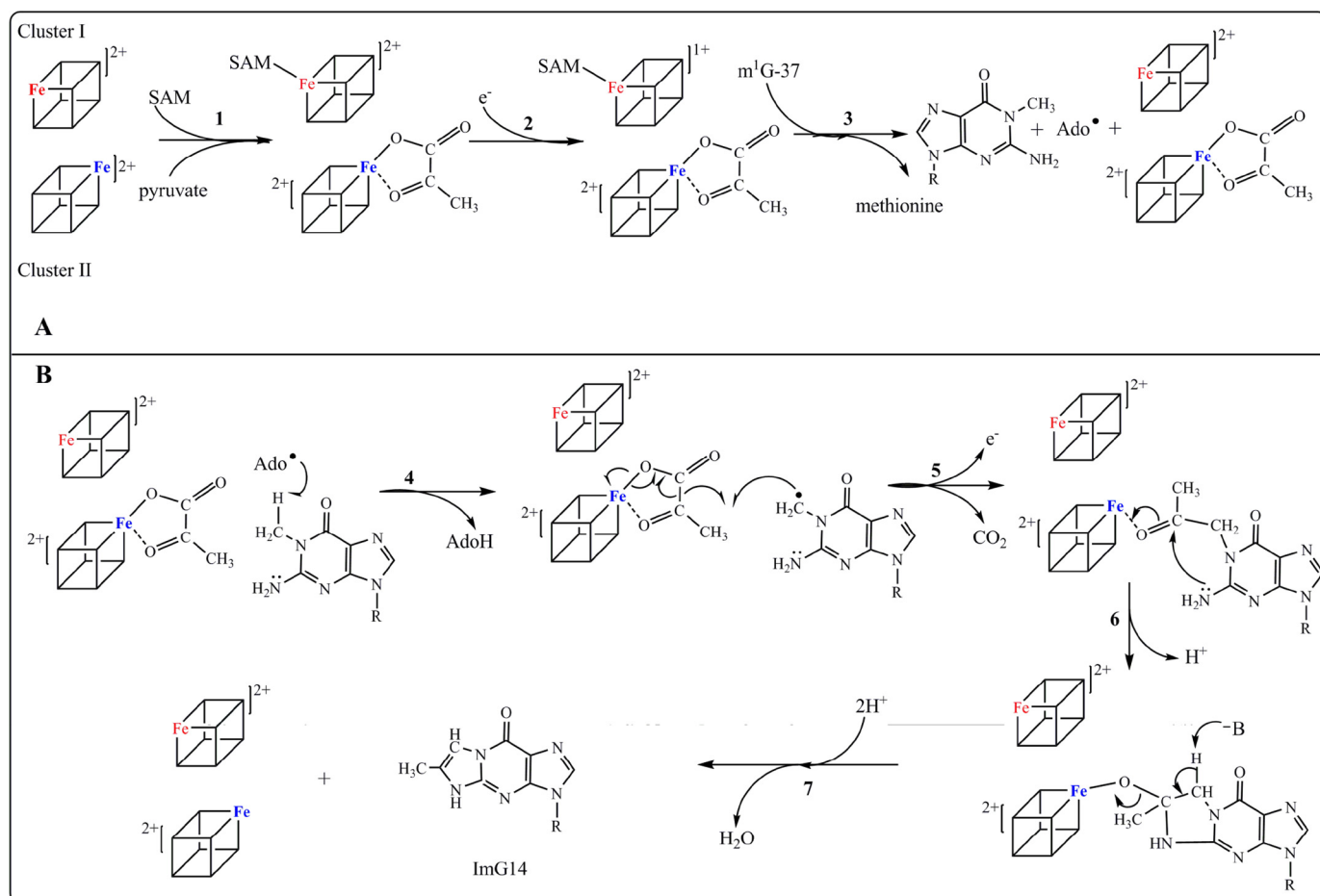
presence of SAM and are present in the control experiment without tRNA (data not shown). *In vitro* production of ImG-14 was monitored as a function of TYW1 protein concentration and reaction time after subtracting the area of the 51.9-min contamination present in the control experiment.

Fig. 9A shows the TYW1 dependence of the reaction with increased formation of ImG-14 as a function of TYW1 concentration. Enzyme concentration dependence was linear up to 5 μ M. Under the same assay conditions described above and by using a concentration of 2 μ M TYW1, the production of ImG-14 was found to be linear for 40 min before reaching a plateau (Fig. 9B).

DISCUSSION

To study the chemistry of the cryptic construction of the tricyclic ring system of wyosine catalyzed by TYW1 enzyme, we prepared the holo-TYW1 from archaeal *P. abyssi* in pure form. The biochemical, analytical, and spectroscopic studies described here demonstrate that holo-TYW1 enzyme belongs to the subclass of Radical-SAM superfamily displaying two [4Fe-4S] clusters. Moreover, it provides evidence for SAM binding to cluster I and pyruvate interaction with cluster II. Although the

visible spectrum of the peak at 51.9 min corresponding to ImG-14. Panel D, shown is a control HPLC chromatogram of digested tRNA (200 μ g) from an *in vitro* assay in the absence of TYW1 30 min at 60 °C. The peak with the asterisk indicates unknown modified nucleoside that elutes at the same retention time as ImG-14. Panel E, shown is a UV-visible spectrum of the contaminant that elutes at the same retention time as ImG-14 product.



SCHEME 2. **Proposed catalytic reaction mechanism of holo-TYW1.** The cubes represent radical-SAM cluster I and cluster II, respectively. Panel A, SAM and pyruvate binding to cluster I and II, respectively (reaction 1) are shown. Reduction of cluster I (reaction 2) is shown. Reductive cleavage of SAM in the presence of m¹G37-tRNA substrate (reaction 3) is shown. Panel B, shown is the proposed mechanism for ImG-14 formation. Ado•, 5'-deoxyadenosyl radical; AdoH, 5'-deoxyadenosine.

current literature on SAM-dependent enzymes hints to the assignment of cluster I as the cluster bound by the CX₃CX₂C motif and, therefore, cluster II as the one bound by the CX₁₂CX₁₂C motif, a definite proof still needs to be provided.

The presence of two [4Fe-4S] clusters in the as-reconstituted protein has been unambiguously evidenced by the EPR study of the reduced protein; the two clusters appear to have slightly different g values and thus can be differentiated with this technique. In contrast, the signals of the two clusters in the oxidized state can be hardly distinguished in Mössbauer spectroscopy, and the presence of two different clusters may be surmised only from the relatively important broad line of the quadrupole doublet. However, both spectroscopies give clear signatures of each cluster upon the addition of the two co-substrates.

SAM addition to the reduced protein drastically changes the shape of the EPR spectrum, and this interaction involves the entire corresponding cluster I. This interaction has been further secured by HYSCORE experiment. In contrast, SAM addition to the holo-TYW1 protein does not affect the Mössbauer spectrum. There are precedents in the literature where this interaction does not strongly disturb the Mössbauer spectrum even though SAM interacts with the oxidized cluster as well (27).

Further addition of pyruvate to SAM-treated reduced holo-TYW1 induces the loss of the EPR signal associated to cluster II due to oxidation as revealed by Mössbauer spectroscopy. This observation and the fact that reduction of cluster II is far slower than that of cluster I could indicate that cluster II has a significantly lower redox potential that is highly sensitive to ligand binding. Whatever the intrinsic cause of the oxidation, cluster II, upon pyruvate addition, exhibits a differentiated iron site that suggests its interaction with pyruvate. After the early work on aconitase (22), the presence of such sites in [4Fe-4S]²⁺ clusters binding a small molecule has been documented in a number of cases (28, 29). This has been interpreted as partial localization of the valences of one delocalized Fe^{II}Fe^{III} pair of the unbound [4Fe-4S]²⁺ cluster, the other pair remaining delocalized (28). This localization produces a (more) ferric and a (more) ferrous component. Only the latter is usually detectable by its high velocity line as found here, the former being hidden behind the doublet of the delocalized pair and here by the doublets associated to the other cluster. Whereas the Mössbauer data clearly show an interaction between the pyruvate substrate and cluster II, it does not strictly demonstrate pyruvate binding to the cluster. Nevertheless, we believe that such binding is likely on the following grounds: (i) the α-ketoacid function of

pyruvate is well documented to chelate iron ions as for example in α -ketoglutarate-dependent non heme iron enzymes (30), (ii) very recent work from Schünemann and co-workers (31) and some of us (29) have definitely established the link between differentiated sites and substrates binding to the $[4\text{Fe-4S}]^{2+}$ cluster.

In the reported *in vitro* assay described by Young and Bandarian (12), the tRNA substrate used for the reaction was obtained from an *in vitro* transcription. This tRNA analog lacks any modification that could be important for the enzyme-substrate interaction and furthermore necessitates in the assay the presence of TRM5 that converts G37-tRNA into $\text{m}^1\text{G37-tRNA}$. Under these conditions the incubation time for the transformation was reported to be 12 h (12).

To simplify the reaction mixture of the assay, we used a tRNA bulk isolated from a strain of *S. cerevisiae* lacking the *tyw1* gene, which accumulates $\text{m}^1\text{G37-tRNA}$, the substrate of TYW1. The use of this substrate facilitates the HPLC analysis of the reaction and allows monitoring of both $\text{m}^1\text{G37-tRNA}$ substrate conversion and ImG-14-tRNA product formation. Indeed, these compounds can be separated by HPLC and identified from their characteristic well defined HPLC retention time, UV-visible, and mass spectrometric properties. Under these conditions the kinetics of the reaction clearly showed that $\text{m}^1\text{G37}$, corresponding to the peak eluted at 32.9 min, could be almost totally converted in 30 min by the enzymatic reaction into the expected ImG-14 product (elution time, 51.9 min).

Finally, our biochemical, analytical, and spectroscopic characterization allows us to end up with a mechanism different from that proposed by Young and Bandarian (12) and provides a rationalization of previously published results that were incompletely understood (13). TYW1 contains six conserved Cys residues organized into two triad motifs (Fig. 1). *In vivo* studies conducted on *S. cerevisiae* showed that substitution of any of these cysteine residues with serine abolishes the activity (13). This is expected for the cysteine belonging to the Radical-SAM triad, but our data showing that the second cysteine triad is engaged into an essential $[4\text{Fe-4S}]$ cluster now explains why mutants of the second triad are also inactive. Moreover, these *in vivo* studies cannot be explained by the mechanism proposed by Young and Bandarian (12). On the contrary, our results strongly support the hypothesis that the holo-TYW1, in accordance with recent findings on other Radical-SAM enzymes (15–17), has evolved two different $[4\text{Fe-4S}]$ clusters for binding and activation of two co-substrates, SAM and pyruvate. On the basis of the present data a proposed mechanism is depicted in Scheme 2. In this model the reaction begins with the formation of the complex resulting from binding of SAM to cluster I and pyruvate to cluster II (Scheme 2A, reaction 1), in agreement with our spectroscopic results (see Figs. 3, B and C, 4, and 5). In the presence of electrons, cluster I-SAM complex is reduced, and cluster II-pyruvate complex remains oxidized (Scheme 2A, reaction 2) as shown by our spectroscopic data (see Figs. 4B and 6). When $\text{m}^1\text{G37-tRNAs}$, the substrate of the reaction, is added to the reaction mixture, the reduced-cluster I-SAM complex undergoes reductive cleavage of SAM to generate the canonical Ado^\bullet radical (Scheme 2A, reaction 3) with concomitant release of methionine. Ado^\bullet initiates H-atom

abstraction from the methyl group of $\text{m}^1\text{G37-tRNA}$ (Scheme 2B, reaction 4), generating a substrate radical, whereas pyruvate remains bound to oxidized cluster II. The addition of this substrate radical to C2 of pyruvate initiates homolytic scission of the C1-C2 bond and elimination of CO_2 and release of one electron (Scheme 2B, reaction 5). The last two steps of the mechanism consist of the formation of the tricyclic ring system through nucleophilic addition of the nitrogen atom on the C3 of pyruvate followed by the release of ImG-14 assisted by general acid-base-catalyzed removal of H_2O (Scheme 2B, reactions 6 and 7). This general acid-base mechanism could rely on the conserved lysine residue, which in the mechanism of Young and Bandarian (12) was proposed to form a Schiff base able to stabilize intermediates of the reaction. Alternatively, reactions 5 and 6 of Scheme 2B could be the other way around (initial nucleophilic attack of the exocyclic G37 amino group on the cluster II-activated carbonyl followed by radical coupling). A number of questions remain unsolved in this model. In particular what the molecular basis of the interaction of cluster II with pyruvate is and how the latter controls its redox potential. Also, another important question is to understand the electron transfer steps. Further experiments with mutant TYW1 devoided of one or another center should help in the understanding of this complex system.

Acknowledgments—We thank Guylaine Miotello, Alain Lorphelin, Cécilia Courbey, Jacques Gaillard (Commissariat à l'Energie Atomique), and Henri Grosjean (CNRS) for preliminary work on *P. abyssi* TYW1. We also thank Thibaut Molle for providing SAM and Patrice Catty for help in yeast culture.

REFERENCES

- Grosjean, H. (ed) (2009) *DNA and RNA Modification Enzymes: Structure, Mechanism, Function and Evolution*, Landes Bioscience, Texas
- Agris, P. F. (1996) The importance of being modified. Roles of modified nucleosides and Mg^{2+} in RNA structure and function. *Prog. Nucleic Acid Res. Mol. Biol.* **53**, 79–129
- Kirino, Y., and Suzuki, T. (2005) Human mitochondrial diseases associated with tRNA wobble modification deficiency. *RNA Biology* **2**, 41–44
- Kirino, Y., Goto, Y., Campos, Y., Arenas, J., and Suzuki, T. (2005) Specific correlation between the wobble modification deficiency in mutant tRNAs and the clinical features of a human mitochondrial disease. *Proc. Natl. Acad. Sci. U.S.A.* **102**, 7127–7132
- Atta, M., Fontecave, M., and Mulliez, E. (2009) in *DNA and RNA Modification Enzymes: Structure Mechanism, Function and Evolution* (Grosjean, H., ed) pp. 347–357, Landes Bioscience, Austin, TX
- Limbach, P. A., Crain, P. F., and McCloskey, J. A. (1994) Summary. The modified nucleosides of RNA. *Nucleic Acids Res.* **22**, 2183–2196
- Waas, W. F., de Crécy-Lagard, V., and Schimmel, P. (2005) Discovery of a gene family critical to wyosine base formation in a subset of phenylalanine-specific transfer RNAs. *J. Biol. Chem.* **280**, 37616–37622
- Urbanavicius, J., Droogmans, L., Armengaud, J., and Grosjean, H. (2009) in *DNA and RNA Modification Enzymes: Structure, Mechanism, Function and Evolution* (Grosjean, H., ed) pp. 423–435, Landes Bioscience, Austin, TX
- de Crécy-Lagard, V., Brochier-Armanet, C., Urbanavicius, J., Fernandez, B., Phillips, G., Lyons, B., Noma, A., Alvarez, S., Droogmans, L., Armengaud, J., and Grosjean, H. (2010) Biosynthesis of wyosine derivatives in tRNA. An ancient and highly diverse pathway in archaea. *Mol. Biol. Evol.* **27**, 2062–2077
- Sofia, H. J., Chen, G., Hetzler, B. G., Reyes-Spindola, J. F., and Miller, N. E. (2001) Radical SAM, a novel protein superfamily linking unresolved steps

- in familiar biosynthetic pathways with radical mechanisms. Functional characterization using new analysis and information visualization methods. *Nucleic Acids Res.* **29**, 1097–1106
11. Fontecave, M., Atta, M., and Mulliez, E. (2004) *S*-Adenosylmethionine. Nothing goes to waste. *Trends Biochem. Sci.* **29**, 243–249
 12. Young, A. P., and Bandarian, V. (2011) Pyruvate is the source of the two carbons that are required for formation of the imidazoline ring of 4-demethylwyosine. *Biochemistry* **50**, 10573–10575
 13. Suzuki, Y., Noma, A., Suzuki, T., Senda, M., Senda, T., Ishitani, R., and Nureki, O. (2007) Crystal structure of the radical SAM enzyme catalyzing tricyclic modified base formation in tRNA. *J. Mol. Biol.* **372**, 1204–1214
 14. Goto-Ito, S., Ishii, R., Ito, T., Shibata, R., Fusatomi, E., Sekine, S. I., Bessho, Y., and Yokoyama, S. (2007) Structure of an archaeal TYW1, the enzyme catalyzing the second step of wye-base biosynthesis. *Acta Crystallogr. D Biol. Crystallogr.* **63**, 1059–1068
 15. Lees, N. S., Hänzelmann, P., Hernandez, H. L., Subramanian, S., Schindelin, H., Johnson, M. K., and Hoffman, B. M. (2009) ENDOR spectroscopy shows that guanine N1 binds to [4Fe-4S] cluster II of the *S*-adenosylmethionine-dependent enzyme MoaA. Mechanistic implications. *J. Am. Chem. Soc.* **131**, 9184–9185
 16. Grove, T. L., Ahlum, J. H., Sharma, P., Krebs, C., and Booker, S. J. (2010) A consensus mechanism for radical SAM-dependent dehydrogenation? BtrN contains two [4Fe-4S] clusters. *Biochemistry* **49**, 3783–3785
 17. Flühe, L., Knappe, T. A., Gattner, M. J., Schäfer, A., Burghaus, O., Linne, U., and Marahiel, M. A. (2012) The radical SAM enzyme AlbA catalyzes thioether bond formation in subtilisin A. *Nat. Chem. Biol.* **8**, 350–357
 18. Fish, W. W. (1988) Rapid colorimetric micromethod for the quantitation of complexed iron in biological samples. *Methods Enzymol.* **158**, 357–364
 19. Beinert, H. (1983) Semi-micro methods for analysis of labile sulfide and of labile sulfide plus sulfane sulfur in unusually stable iron-sulfur proteins. *Anal. Biochem.* **131**, 373–378
 20. Gehrke, C. W., and Kuo, K. C. (1989) Ribonucleoside analysis by reversed phase high performance liquid chromatography. *J. Chromatogr.* **471**, 3–36
 21. Tyryshkin, A. M., Dikanov, S. A., Reijerse, E. J., Burgard, C., and Huttermann, J. (1999) Characterization of bimodal coordination structure in nitrosyl heme complexes through hyperfine couplings with pyrrole and protein nitrogens. *J. Am. Chem. Soc.* **121**, 3396–3406
 22. Emptage, M. H., Kent, T. A., Kennedy, M. C., Beinert, H., and Münck, E. (1983) Mössbauer and EPR studies of activated aconitase. Development of a localized valence state at a subsite of the [4Fe-4S] cluster on binding of citrate. *Proc. Natl. Acad. Sci. U.S.A.* **80**, 4674–4678
 23. Gambarelli, S., Luttringer, F., Padovani, D., Mulliez, E., and Fontecave, M. (2005) Activation of the anaerobic ribonucleotide reductase by *S*-adenosylmethionine. *ChemBiochem.* **6**, 1960–1962
 24. Chandor, A., Douki, T., Gasparutto, D., Gambarelli, S., Sanakis, Y., Nicolet, Y., Ollagnier-De-Choudens, S., Atta, M., and Fontecave, M. (2007) Characterization of the DNA repair spore photoproduct lyase enzyme from *Clostridium acetobutylicum*. A radical-SAM enzyme. *Comptes Rendus Chimie* **10**, 756–765
 25. Chen, D., Walsby, C., Hoffman, B. M., and Frey, P. A. (2003) Coordination and mechanism of reversible cleavage of *S*-adenosylmethionine by the [4Fe-4S] center in lysine 2,3-aminomutase. *J. Am. Chem. Soc.* **125**, 11788–11789
 26. Kasai, H., Goto, M., Ikeda, K., Zama, M., Mizuno, Y., Takemura, S., Matsuura, S., Sugimoto, T., and Goto, T. (1976) Structure of wye (Yt base) and wyosine (Yt) from *Torulopsis utilis* phenylalanine transfer ribonucleic acid. *Biochemistry* **15**, 898–904
 27. Cospér, M. M., Jameson, G. N., Davydov, R., Eidsness, M. K., Hoffman, B. M., Huynh, B. H., and Johnson, M. K. (2002) The [4Fe-4S]²⁺ cluster in reconstituted biotin synthase binds *S*-adenosyl-L-methionine. *J. Am. Chem. Soc.* **124**, 14006–14007
 28. Seemann, M., Janthawornpong, K., Schweizer, J., Böttger, L. H., Janoschka, A., Ahrens-Botzong, A., Tambou, E. N., Rotthaus, O., Trautwein, A. X., and Rohmer, M. (2009) Isoprenoid biosynthesis via the MEP pathway: in vivo Mössbauer spectroscopy identifies a [4Fe-4S]²⁺ center with unusual coordination sphere in the LytB protein. *J. Am. Chem. Soc.* **131**, 13184–13185
 29. Chan, A., Clemancey, M., Mouesca, J. M., Amara, P., Hamelin, O., Latour, J. M., and Ollagnier de Choudens, S. (2012) Studies of inhibitor binding to the [4Fe-4S] cluster of quinolinate synthase. *Angew. Chem. Int. Ed. Engl.* **51**, 7711–7714
 30. Loenarz, C., and Schofield, C. J. (2008) Expanding chemical biology of 2-oxoglutarate oxygenases. *Nat. Chem. Biol.* **4**, 152–156
 31. Ahrens-Botzong, A., Janthawornpong, K., Wolny, J. A., Tambou, E. N., Rohmer, M., Krasutsky, S., Poulter, C. D., Schünemann, V., and Seemann, M. (2011) Biosynthesis of isoprene units. Mössbauer spectroscopy of substrate and inhibitor binding to the [4Fe-4S] cluster of the LytB/IspH enzyme. *Angew. Chem. Int. Ed. Engl.* **50**, 11976–11979